A Study on Thermal Resistance over a Solid-Liquid Interface by the Molecular Dynamics Method *

Shigeo MARUYAMA† and Tatsuto KIMURA†

Abstract

Through molecular dynamics simulations, it was demonstrated that a thermal resistance cannot be neglected over a solid-liquid interface when a system size is very small, i.e. the relative importance of thermal resistance of heat conduction is small. A quasi-steady non-equilibrium heat-transfer simulation was performed with the molecular dynamics method. A vapor region was sandwiched between liquid layers, which were in contact with two solid walls. While independently controlling temperatures at ends of walls by the phantom method, the energy flux through the system was accurately calculated. The measured temperature distribution normal to interfaces showed a distinctive jump near the solid-liquid interface, which could be regarded as the thermal resistance over the interface. The thermal resistance was measured for various interaction potential parameters between solid and liquid molecules so that a wide range of wettability could be covered. The thermal resistance was equivalent to 5~20 nm thickness of liquid heat conduction layer, and was strongly dependent on the wettability.

Key Words: *Molecular Dynamics Method, Liquid-Solid Interface, Thermal Resistance, Lennard-Jones*

Nomenclature

e^i	=	energy of a molecule *i*
k	=	spring constant
k_B	=	Boltzmann constant
L_R	=	thermal resistance thickness
M	=	mass flux
m	=	mass
N	=	number of molecules
q	=	heat flux
R_T	=	thermal resistance
r	=	distance of two molecules
T	=	temperature
T_{JUMP}	=	temperature jump
V	=	volume
v_z^i	=	z-directional velocity of molecule *i*
$<v_z>$	=	average of z-directional velocity
z	=	coordinate normal to the interface
α	=	damping factor
Δt	=	time step
ε	=	energy parameter of Lennard-Jones potential
λ	=	heat conductivity
ϕ	=	potential function
θ	=	contact angle
σ	=	length parameter of Lennard-Jones potential
σ_F	=	standard deviation of exciting force

Sub/Superscripts

AR	=	argon
cond	=	condensation side
evap	=	evaporation side
INT	=	between argon and solid molecules
L	=	liquid
S	=	solid
SURF	=	integration of surface molecules
V	=	vapor
W	=	solid wall

1 Introduction

The thermal resistance over solid-solid contact interface has been extensively studied in macroscopic heat transfer field. The thermal conductance over the

* Received: October 30, 1998, Editor: Susumu KOTAKE

† Department of Mechanical Engineering, The University of Tokyo (7-3-1 Hongo, Bunkyo-ku, Tokyo, 113-8656, JAPAN, Tel. (03)-5800-6983)

interface is usually expressed as the sum of solid heat conduction through the true contact area and heat conduction through the gas in the gap. On the other hand, it is usually not necessary to consider the thermal resistance over solid-liquid contact interface for a macroscopic system. When the system size is microscopic as in thin film composites, however, the small thermal resistance due to molecular level ordering is noticeable even for the perfect solid-solid contact [1]. Likewise, the very small liquid-solid contact thermal resistance may be significant at some small system size because the thermal resistance by heat conduction monotonically decreases with the reduction of the system size. A considerable temperature jump over a liquid and solid interface was actually suggested in our molecular dynamics simulation [2]. The temperature jump was considered to arise from the difference of vibrational frequency range of solid and liquid molecules or from the layered structure of liquid molecules just on a solid surface.

The solid-liquid thermal resistance may be understood as an analogy to the temperature jump concept between solid surface and rarefied gas in a certain range of Knudsen number. Although the value of Knudsen number increases with the reduction of a system size, it is not appropriate to apply theories of rarefied gas to liquid. In order to evaluate the contact thermal resistance over a liquid-solid interface, a non-equilibrium molecular dynamics simulation was performed.

2 Molecular Dynamics Method

Fig. 1 shows the system configuration to be simulated. Solid walls were symmetrically arranged to the top and the bottom with liquid regions in contact with them, and the saturated vapor occupied the central region. Lennard-Jones molecules were employed for liquid and vapor with the potential function

$$\phi(r) = 4\varepsilon\left\{(\sigma/r)^{12} - (\sigma/r)^{6}\right\}. \qquad (1)$$

Here, we used the smooth cut-off [3] at 3.5Å as in our simulations of vapor bubble nucleation [4]. For the sake of physical understandings, the L-J molecules were assumed to be argon with potential parameters: m_{AR} = 6.636×10^{-26} kg, σ_{AR} = 3.40 Å and ε_{AR} = 1.67×10^{-21} J.

The solid wall was represented by 3 layers of fcc (111) surface of harmonic molecules (440 molecules per layer). Here, it was set as: mass m_S = 3.24×10^{-25} kg, distance of nearest neighbor molecules σ_S = 2.77 Å, the spring constant k = 46.8 N/m, from physical properties of solid platinum crystal. However, it should be noticed that the solid wall was regarded as electrically insulating material, by neglecting the heat conduction through free electrons. The potential function between solid and argon molecules was also represented by Lennard-Jones

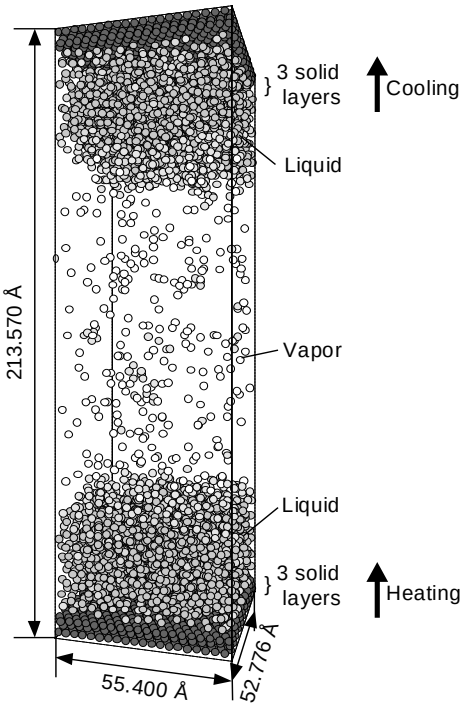

Fig. 1 A snapshot of quasi-steady heat transfer system

function with the length parameter σ_{INT} and the energy parameter ε_{INT}. The length parameter was kept constant as $\sigma_{INT} = (\sigma_S + \sigma_{AR}) / 2$ = 3.085 Å based on the simple combination rule. On the other hand, the energy parameter ε_{INT} was varied in the range of 0.527×10^{-21} to 1.169×10^{-21} J, in order to change the wettability of the liquid to the wall [2, 4] (See Table 1 and Fig. 2). From our previous molecular dynamics simulations of liquid droplet in contact with a surface [2,5] and vapor bubble on surface [4], the wettability of liquid to the surface could be estimated. The range of contact angle varied from about 105° to 0° (super-hydrophilic).

The temperature of the solid surface was controlled by a layer of phantom molecules outside of 3 layer solid walls. The phantom molecules modeled the infinitely wide bulk solid kept at a constant temperature T with the proper heat conduction characteristics [6,7]. In practice, a solid molecule in the 3rd layer was connected to a phantom molecule with a spring of $2k$ and a damper of α = 5.184×10^{-12} kg/s in vertical direction and with springs of $3.5k$ and dampers of α in two horizontal directions. A phantom molecule was further excited by the random force of gaussian distribution with the standard deviation

$$\sigma_F = \sqrt{\frac{2\alpha k_B T}{\Delta t}}\,. \qquad (2)$$

The energy flux to the calculation system was accurately calculated by integrating the exciting force and the damping force applied to the phantom molecules

Table 1 Simulation conditions and measured values. See Fig. 2 and text for nomenclature.

Label		ε_{INT} ($\times 10^{-21}$ J)	q_W (MW/m^2)	T_{JUMP} (K)	R_T (m^2·K/W)	λ_L (W/m·K)	L_R (nm)	dN_L/dt (1/ns)	q_V (MW/m^2)	M (kg/m^2·s)
E2	evap	0.527	34.0	8.45	0.249×10^{-6}	0.072	20.3	-119	10.7	254
	cond		31.3	6.32	0.202×10^{-6}	0.065	16.5	119		
E3	evap	0.688	55.3	5.98	0.108×10^{-6}	0.103	8.8	-214	20.3	489
	cond		60.3	5.90	0.098×10^{-6}	0.079	8.0	208		
E4	evap	0.848	65.3	5.76	0.088×10^{-6}	0.091	7.2	-248	19.2	541
	cond		64.8	4.91	0.076×10^{-6}	0.086	6.2	249		
E5	evap	1.009	72.3	4.62	0.064×10^{-6}	0.052	5.2	-273	24.9	569
	cond		74.1	4.32	0.058×10^{-6}	0.072	4.8	268		
E6	evap	1.169	89.7	4.87	0.054×10^{-6}	0.100	4.4	-330	28.5	725
	cond		90.5	3.67	0.041×10^{-6}	0.097	3.3	321		

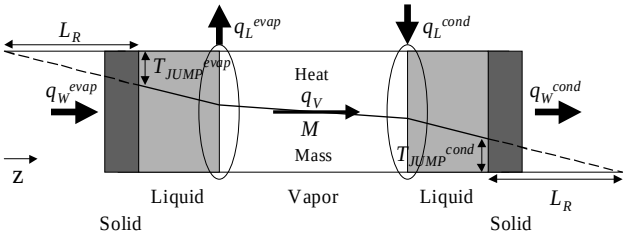

Fig. 2 A schematic of heat balance of the system

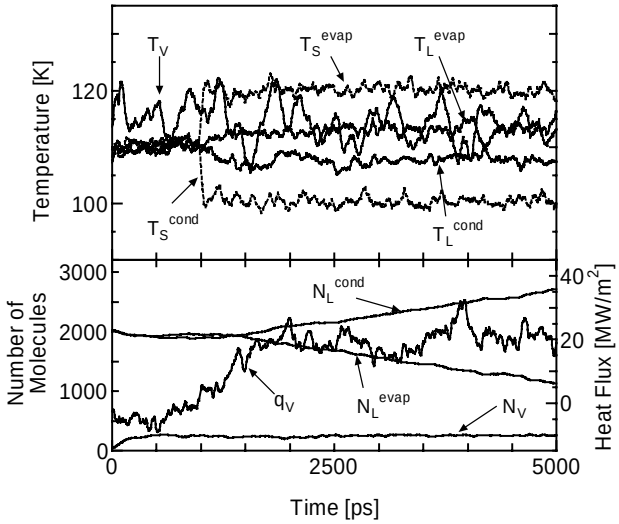

Fig. 3 Temperature, number of molecules and heat flux variations for E3.

since the total energy of the system was conserved without these artificial forces. In our preliminary simulations, it was confirmed that the sum of the total energy and the integration of net energy flow through phantom molecules was exactly kept constant by using a careful integration technique.

The central vapor region of the system may seem to be unnecessary for the measurement of liquid-solid contact thermal resistance. The purpose of this saturated vapor region was to guarantee that the pressure of the system was in the saturated condition, since the pressure measurement and control were generally not straightforward [4]. Furthermore, this system configuration could be used for the consideration of the liquid-vapor interface in future.

The simulation system size was set to be $55.4 \times 52.8 \times 213.6$ Å as shown in Fig. 1 with periodic boundary conditions for four side directions. Initially, argon molecules of 2048 were located in contact to both walls as a fcc crystal. During the initial 500 ps of a simulation, the velocity-scaling temperature control was used for all molecules to the set temperature of 110 K. The equilibrium condition was obtained by controlling only phantom molecules for following 500 ps. At 1000 ps, the temperature of the evaporation side and the condensation side was set to 120 K and 100 K, respectively, by the phantom method. The Verlet integration was used with the time interval of Δt = 5 fs.

3 Results and Discussions

The upper panel in Fig. 3 shows the time history of solid surface temperatures T_S^{evap} & T_S^{cond}, the liquid temperatures T_L^{evap} & T_L^{cond} and the vapor temperatures T_V^{evap} & T_V^{cond} at evaporation (evap) and condensation (cond) sides for the case of E3. The lower panel illustrates the heat flux q_V normal to the interfaces measured at the 50 Å thick central vapor region and number of molecules of vapor N_V and liquids N_L. At 1000 ps, the system was almost in equilibrium at temperature of 110 K. Number of liquid molecules at both sides N_L^{evap} & N_L^{cond} and number of vapor molecules were self-adjusted for the saturated condition, while q_V was settled to 0.

As the temperature difference in both ends of walls was suddenly applied at 1000 ps, solid wall temperature T_S^{evap} and T_S^{cond} quickly responded to be about the set

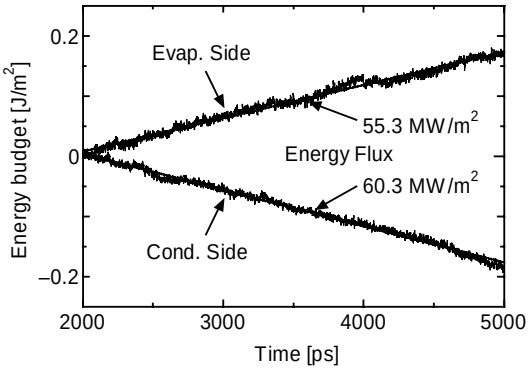

Fig. 4 Energy budget of phantom control for E3.

temperatures 120 K and 100 K, respectively. The change in the liquid temperature followed and they reached almost the constant values after about 500 ps. The heat flux q_V slowly increased until 2000 ps and finally reached a constant value about 20 MW/m^2. Then, number of liquid molecules N_L^{evap} at evaporation side began to decrease and that at condensation side N_L^{cond} began to increase at almost the same rate, keeping the number of vapor molecules N_V unchanged. Here, the linear change of N_L^{evap} and N_L^{cond} after about 2000 ps was used to calculated the phase-change rate dN_L/dt listed in Table 1.

Fig. 4 shows the integration of heat flux $q_w\,dt$ from 2000 ps, which was directly measured by the integration of forces on the phantom molecules. The integrated heat flux on both sides can be perfectly fit to linear lines and the constant heat flux q_W^{evap} and q_W^{cond} can be measured as 55.3 MW/m^2 and 60.3 MW/m^2, respectively. These two heat fluxes can be regarded as almost the same value (see other conditions in Table 1). Hence, this heat transfer system can be regarded as quasi-steady state from about 2000 ps to 5000 ps, where a constant heat flux penetrated the whole system and steady temperature distribution was achieved with the same rate of evaporation and condensation in two liquid-vapor interfaces.

The density distribution, the temperature distribution and the z-directional velocity distribution normal to interfaces were averaged from 2000 ps to 5000 ps in Fig. 5. Since the position of liquid-vapor interfaces changed in time, the short time averages for 100 ps at 2000, 3500 and 5000 ps for the density distribution are also plotted in Fig. 5. The instantaneous density distribution should be a bit sharper than these time-averaged distributions. Temperature for solid molecules was measured as the average of each layer and expressed as dots in Fig. 5. The temperature distribution clearly shows the discontinuity at the solid liquid interface. The temperature distribution in liquid region was fit to a linear line in Fig. 5 to obtain the temperature jump at the interface T_{JUMP}.

The thermal resistance R_T was determined from the

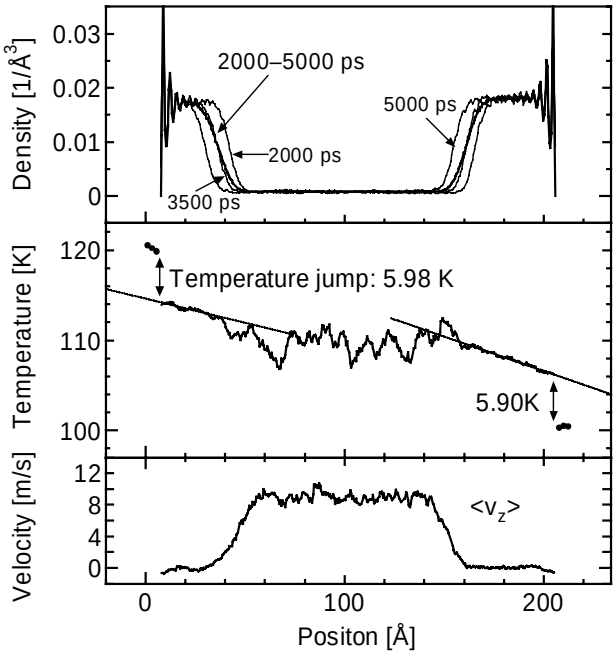

Fig. 5 Density, temperature, and velocity distributions.

temperature jump T_{JUMP} and the heat flux q_W as $R_T = T_{JUMP}/q_W$ (listed in Table 1). The heat conductivity λ_L was calculated from the heat flux q_W and the temperature gradient in liquid regions, simply as $\lambda_L = q_W/(\partial T/\partial z)$. Even though there were considerable fluctuations in the measured heat conductivity listed in Table 1, the simple average of 0.082 W/m·K was the best estimate from these simulations with the assumption that the Fourier's law was valid. This value was actually in good agreement with the macroscopic value of liquid argon: 0.097 W/m·K at the saturated temperature of 110 K [8]. In order to express the physical meaning of the amount of the thermal resistance R_T, the equivalent liquid-heat-conduction length was defined as $L_R = \lambda_L \cdot R_T$. This length can be regarded as the equivalent thickness of the liquid heat-conduction layer that has the same amount of thermal resistance (see Fig. 2). When this "thermal resistance thickness R_T" is not negligible compared to the system size, the effect of the thermal resistance is not negligible compared to the heat conduction resistance through the liquid layer.

The temperature distribution in the vapor region had large fluctuations because the number of molecules is relatively small. However, it is clear that the temperature gradient in vapor region is less than liquid region even though the heat conductivity of argon vapor is expected to be about 1/10 of that of argon liquid. This large conductivity through the gas region is ascribed to the net molecular flux $\langle v_Z \rangle$ in Fig. 5 (the mass flow rate M in Table 1).

As the z-directional velocity v_z^i is decomposed to $v_z^i = \langle v_z \rangle + v'^i_z$, then the heat flux q_v in z-direction can be approximated as

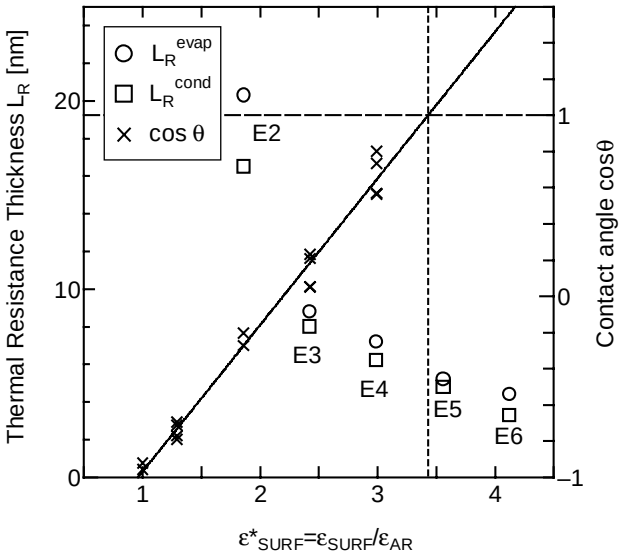

Fig. 6 Thermal resistance thickness and contact angle.

$$q_V = \frac{1}{V}\sum_{i\in V} e^i v_z{}^i = \frac{1}{V}\frac{3}{2}k_B TN\langle v_z\rangle + \frac{1}{V}\sum_{i\in V} e^i v'_z{}^i \qquad (3)$$

where e^i is the total energy of molecule i and V is the volume of measuring control volume. Since the measurement was done in vapor region, the potential energy contribution to e^i was neglected in RHS. The first and second term in RHS represents the energy flux due to the net mass flux and the heat flux due to the vapor heat conduction, respectively. The first term was predominant in these simulations.

It should be noticed that when the vaporization coefficient or condensation coefficient is considered for a non-equilibrium liquid-vapor interface, effect of this net mass flux must be removed. It seems that a considerably large vapor region should be necessary for the simply calculation system of such purpose.

The overall heat balance is schematically summarized in Fig. 2. The heat flux through the vapor region q_V was roughly 1/3 of the heat flux through wall q_W as listed in Table 1. The heat flux through higher temperature side $q_W{}^{evap}$ was consumed for the latent heat of the evaporation and residual heat flux q_V was mostly carried by the net mass flux through the vapor region. The latent heat of condensation was added to q_V to reproduce $q_W{}^{cond}$ at the lower temperature side.

Fig. 6 shows the dependency of the thermal resistance thickness L_R on the potential parameter between solid and liquid molecules. Our previous studies of liquid droplet in contact with the solid surface [2, 5] showed that the cosine of contact angle was expressed by a linear function of the depth of integrated surface potential ε_{SURF} as shown in Fig. 6. In this report, only the energy scale ε_{INT} of the interaction potential was varied in the range as shown in Fig. 6, which was equivalent to the contact angle of about 105° to well beyond 0° (super-hydrophilic condition). The thermal resistance thickness sharply decreased as the wettability increased. However, the thickness kept a finite value of about 5 nm even for the super-hydrophilic condition (θ = 0°). The slight difference of L_R between evaporation and condensation sides was probably due to the temperature difference of about 20 K. Although simulations were performed only for the limited conditions of solid potential parameters and interaction parameters, the rough estimate of the order of the thermal resistance over a solid-liquid interface was obtained. Even though this thermal resistance thickness might be regarded as small enough for most of practical applications, it cannot be always negligible for microscopic systems. Especially for heat transfer measurements using the molecular dynamics simulations, this thermal resistance is usually crucial.

4 Conclusions

A quasi-steady non-equilibrium molecular dynamics simulation was performed in order to measure the contact thermal resistance over solid-liquid interface. A vapor region was sandwiched between liquid layers, which were in contact with two solid walls. Temperatures at ends of two solid walls were controlled by the phantom molecules with the accurate measurement of net energy input or output. The measured temperature distribution along the axis normal to interfaces showed a clear temperature jump at the solid-liquid interface, which was regarded as the thermal resistance over the interface. The thermal resistance was measured for various interaction potential parameters between solid and liquid molecules so that a wide range of wettability could be covered. In the range of the contact angle of 0° (super-hydrophilic) to 105°, thermal resistance was equivalent to 5 ~ 20 nm thickness of liquid-heat-conduction layer. The thermal resistance thickness sharply increased with the decrease of surface wettability. The contact resistance over solid-liquid interface cannot be neglected when this thickness cannot be neglected compared to the system size.

Acknowledgement

The authors gratefully acknowledge efforts of our students, Mr. Soon-Ho Choi and Mr. Koji Yasui during this study.

References

[1] Lee, S.-M., Matamis, G., Cahill, D. G, and Allen, W. P., "Thin-Film Materials and Minimum Thermal Conductivity," Microscale Thermophysical Engineering, 2-1 (1998), 31-36.
[2] Maruyama, S., Kurashige, T., Matsumoto, S.,

Yamaguchi, Y., and Kimura, T., "Liquid Droplet in Contact with a Solid Surface," Microscale Thermophysical Engineering, 2-1 (1998), 49-62.

[3] Stoddard, S. D. and Ford, J., "Numerical Experiments on the Stochastic Behavior of a Lennard-Jones Gas System," Phys. Rev. A, 8, (1973), 1504-1512.

[4] Maruyama, S. and Kimura, T. "A Molecular Dynamics Simulation of a Bubble Nucleation on Solid Surface," Proc. 5th ASME/JSME Thermal Engng. Conf., San Diego, (1999), AJTE99-6511 in press.

[5] Matsumoto, S., Maruyama, S., and Saruwatari, H., "A Molecular Dynamics Simulation of a Liquid Droplet on a Solid Surface," Proc. 4th ASME/JSME Thermal Engng. Conf., 2, (1995), 557-562.

[6] Tully, J. C., "Dynamics of Gas-Surface Interactions: 3D Generalized Langevin Model Applied to fcc and bcc Surfaces," J. Chem. Phys., (1980), 73-4, 1975-1985.

[7] Blömer, J. and Beylich, A. E., "MD-Simulation of Inelastic Molecular Collisions with Condensed Matter Surfaces," Proc. of International Symposium on Rarefield Gas Dynamics, (1996), 392-397

[8] Handbook of Heat Transfer, Japan Society of Mechanical Engineers, (1991).